Research in Astron. Astrophys. **2013** Vol. **13** No. **1**, 15 – 27
http://www.raa-journal.org *http://www.iop.org/journals/raa*

***R**esearch in*
***A**stronomy and*
***A**strophysics*

A multi-wavelength study of the gravitational lens COSMOS J095930+023427 *

Shuo Cao[1,2], Giovanni Covone[2,3], Maurizio Paolillo[2,3] and Zong-Hong Zhu[1]

[1] Department of Astronomy, Beijing Normal University, Beijing 100875, China; *zhuzh@bnu.edu.cn*
[2] Dipartimento di Scienze Fisiche, Università di Napoli "Federico II," Complesso Universitario di Monte S. Angelo, via Cinthia, 80126 Napoli, Italy
[3] INFN, Sezione di Napoli, Complesso Universitario di Monte S. Angelo, via Cinthia, 80126 Napoli, Italy

Received 2012 June 7; accepted 2012 September 12

Abstract We present a multi-wavelength study of the gravitational lens COSMOS J095930+023427 ($z_{\rm l} = 0.892$), together with the associated galaxy group along the line of sight located at $z \sim 0.7$, and the lensed background galaxy. The source redshift is currently unknown, but estimated to be at $z_{\rm s} \sim 2$. This analysis is based on publicly available HST, Subaru and Chandra imaging data, as well as VLT spectroscopy. The lensing system is an early-type galaxy showing a strong [OII] emission line, and produces four bright images of the distant background source. It has an Einstein radius of $0.79''$, about four times larger than the effective radius. We perform a lensing analysis using both a singular isothermal ellipsoid and a peudo-isothermal elliptical mass distribution for the lensing galaxy, and find that the final results on the total mass, the dark matter (DM) fraction within the Einstein radius and the external shear due to a foreground galaxy group are robust with respect to the choice of the parametric model and the source redshift (yet unknown). We measure the luminous mass from the photometric data, and find the DM fraction within the Einstein radius $f_{\rm DM}$ to be between 0.71 ± 0.13 and 0.79 ± 0.15, depending on the unknown source redshift. Meanwhile, the non-null external shear found in our lensing models supports the presence and structure of a galaxy group at $z \sim 0.7$, and an independent measurement of the 0.5–2 keV X-ray luminosity within $20''$ around the X-ray centroid provides a group mass of $M = (3 - 10) \times 10^{13}\ M_{\odot}$, in good agreement with the previous estimate derived through weak lensing analysis. Finally, by inverting the HST/ACS I_{814} image with the lensing equation, we obtain the reconstructed image of the magnified source galaxy, which has a scale of about 3.3 kpc at $z_{\rm s} = 2$ (2.7 kpc at $z_{\rm s} = 4$) and the typical disturbed disk-like appearance observed in low-mass star-forming galaxies at $z \sim 3$. However, deep, spatially resolved spectroscopic data for similar lensed sources are still required to detect the first stage of galaxy evolution, since the available spectrum shows no clear features due to the background source.

Key words: galaxies: individual (COSMOS J095930+023427) — gravitational lensing — dark matter

∗ Supported by the National Natural Science Foundation of China.

1 INTRODUCTION

Since the discovery of the first gravitational lens by Walsh et al. (1979), strong gravitational lensing (GL) has developed into an important astrophysical tool. It is nowadays a primary technique to probe the spatial distribution of dark matter (DM) in cosmic structures (on scales from galaxies to galaxy clusters, e.g. Massey et al. 2010), to investigate the properties and nature of DM (e.g. Grin et al. 2007; Moustakas et al. 2009), to study in great detail the faint population of high-redshift galaxies (e.g. Richard et al. 2008; Monna & Covone 2012), and to provide a measurement of the Hubble constant, which is free of effects from calibration in the cosmic distance ladder (e.g. Schechter 2005) or cosmological parameters via statistical analysis (see, e.g., Cao & Zhu 2012; Cao et al. 2012 and references therein).

Compared with other observational techniques to probe the radial mass profile, such as kinematics of stellar populations (Cappellari et al. 2006; van der Wel & van der Marel 2008) and the temperature of X-ray emitting gas (Humphrey et al. 2006; Churazov et al. 2008), the advantage of GL lies in its ability to investigate the total mass within the Einstein radius without any assumptions about the dynamical state of the system. Moreover, about two hundred new strong galaxy-galaxy lenses, in which the lensed sources are extended galaxies, have been discovered by recent large systematic surveys such as the SDSS survey (SLACS: Bolton et al. 2006, 2008; Allam et al. 2007), the CFHTLS surveys (SL2S: Cabanac et al. 2007), and the COSMOS survey (Faure et al. 2008; Jackson 2008). These valuable samples can be used not only to study the DM in the lensing galaxies, but also to study the properties of high-redshift ($z \sim 2$) star-forming galaxies acting as sources.

Insights into the structure of galaxies are emerging from two aspects of these works. One is the joint statistical analysis for a large sample of galaxy-scale lenses. The DM content in the central regions for early-type galaxies has been extensively investigated by Cappellari et al. (2006); Tortora et al. (2009), who found that the central DM fraction is an increasing function of the total mass. Recently, by combining strong and weak GL, Lagattuta et al. (2010) have measured the average mass properties of a sample of 41 strong gravitational lenses at a moderate redshift, and found that changing the inner slope of the DM profile by $\sim 20\%$ will yield a $\sim 30\%$ change in the stellar mass-to-light ratio. The other is mapping the mass distribution of individual galaxy-scale lens systems. Covone et al. (2009) analyzed the total mass and the DM fraction within the Einstein radius for a $\sim L^*$ S0 galaxy at $z = 0.4656$ as a function of the lensed source redshift, and obtained some results supporting the above mentioned statistical study at a lower scale for galaxy mass.

Meanwhile, the properties and mass distribution of high-redshift galaxies in the distant Universe ($z > 2 - 3$) still represent almost completely uncharted territory. A detailed exploration of more high$-z$ galaxies by means of lensing magnification would give great insight into the first stages of galaxy formation.

In this paper, we present an analysis of the gravitational lens COSMOS 095930+023427, an early-type lensing galaxy at $z_{\rm l} = 0.8923 \pm 0.0007$ (COSMOS J095930+023427), discovered in the field of the Cosmic Evolution Survey (COSMOS, Scoville et al. 2007) by Jackson (2008), through a systematic, visual inspection of lensing candidates. The aim of the present paper is to present a multi-wavelength study of this galaxy-scale gravitational lens, focusing on probing the DM distribution in the inner regions of a $z \sim 0.8$ elliptical galaxy and the properties of the lensed background source.

The lensing system is clearly a four-image gravitational lens system (see Fig. 1), with two merging images lying about $0.8''$ from the lensing galaxy and two other images near it toward the southeast and southwest. The Subaru color imaging clearly shows that the lensed images have a similar blue color, and the lensing galaxy dominates the light in the I band, but it is hardly detectable in the B image (Fig. 1).

One important feature of J095930+023427 is that the lensing galaxy is bright and well separated from the lensed HST images, which makes it possible to acquire a good determination of its photometric properties. Deriving information on both the mass and the light properties of this elliptical

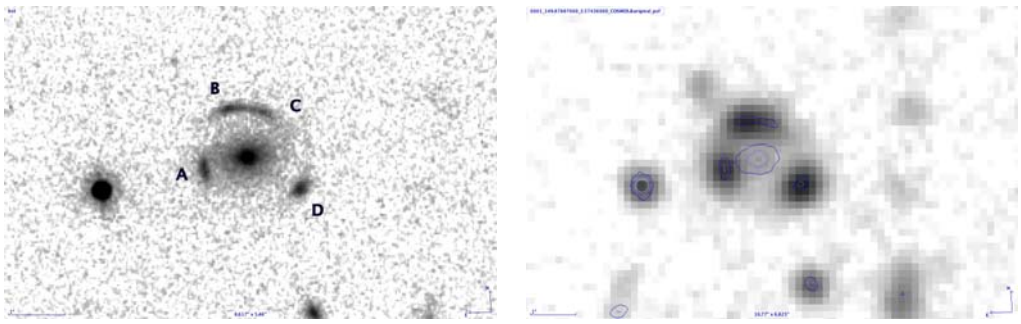

Fig. 1 Images of the GL system with the identification of the four lensed images. *Left panel*: HST/ACS I_{814} data. *Right panel*: B-band SUBARU data, with contours of the sources from the HST/ACS data. The field of view is $10'' \times 7''$.

galaxy allows us to probe its DM fraction ($f_{\rm DM}$), defined as $f_{\rm DM} = 1 - M_\star/(M_\star + M_{\rm DM})$. A study of the lensing galaxy was presented by Faure et al. (2011), who used a singular isothermal ellipsoid (SIE) model for the lensing galaxy and took into account the presence of a lower-redshift galaxy cluster along the line of sight. They obtained a DM fraction within the Einstein radius of $f_{\rm DM} = 0.71^{+0.30}_{-0.12}$.

The goal of the present paper is to present a detailed multi-wavelength study of this lens, including an improved lensing model based on the rich data set obtained by the COSMOS collaboration for the lensing galaxy as well as new insights into the mass distribution of the lensed young galaxy at $z \sim 2$. This paper is organized as follows. In Section 2, we present HST imaging and Subaru spectroscopic observations of the lens systems. In Section 3, we introduce the strong-lens mass models and present results of the constraint on the lensing galaxy. In Section 5, we briefly describe the light properties of a non-local elliptical galaxy and its corresponding DM fraction. Section 6 shows the main properties of the reconstructed source galaxy. Discussion and conclusions appear in Section 7. Throughout this work, we assume a flat cosmology with $\Omega_{\rm m} = 0.3$, $\Omega_\Lambda = 0.7$ and $H_0 = 70$ km s^{-1} Mpc^{-1}. The age of the Universe at the redshift of the lens is 6.2 Gyr. All magnitudes presented in this paper are given in the AB system.

2 THE DATA

In this section, we present the imaging and spectroscopic data used in the analysis of COSMOS 095930+023427. The system was imaged as a part of the large observational effort to cover the COSMOS field. In our analysis, we use the imaging data from HST/ACS, Subaru/Suprime-Cam, *XMM*, *Chandra* and spectroscopic data from zCOSMOS (Lilly et al. 2009). A full description of the available dataset is given in Scoville et al. (2007), and here we give only a brief summary.

HST high-resolution images are essential to build an accurate model of the gravitational lens, while the large multi-wavelength coverage allows us to constrain the redshift and the stellar population of the lensing galaxy and the lensed source. We obtain our data thorough the COSMOS Cutouts service[1]. HST/ACS images cover a square field of about 1.8 deg^2. The final data have a scale of $0.03''$ per pixel, with a depth of $I_{814} \simeq 28$ mag and $\sim$50% completeness for sources $0.5''$ in diameter at $I_{814} = 26.0$ mag. Subaru data are obtained in six broad-band filters (B, g', V, r', i', z') and one narrow-band (NB816) filter (Taniguchi et al. 2007). The Subaru color imaging clearly shows

[1] Website: *http://irsa.ipac.caltech.edu/data/COSMOS/index_cutouts.html*

that the lensed images have a similar blue color and the lensing galaxy dominates the light in the I band.

The lensing galaxy was selected among the spectroscopic targets of the zCOSMOS project (Lilly et al. 2009). We retrieved the spectra from the second data release, containing the zCOSMOS-bright spectroscopic observations that were carried out using VLT/VIMOS. The measured redshift is $z_{\rm l} = 0.8923 \pm 0.0007$, classified as a probable redshift in Lilly et al. (2009). The redshift measurement is mostly based on the robust identification of the [OII] emission line and a weak CaII-K absorption feature. Unfortunately, the VLT spectrum shows no signature from the background source; as discussed hereafter, we can rely only on the available photometric data to constrain its redshift.

The main arc (as seen in merging images B and C) is located at about $0.85''$ from the center of the main galaxy. A first model of this system was presented by Faure et al. (2011). They estimated the Einstein radius to be $R_{\rm E} = 0.79'' \pm 0.02''$ (Faure et al. 2011). This corresponds to a linear scale of 6 kpc. In the following, we constrain the total mass and dark matter fraction of the galaxy, using the Faure et al. value of $R_{\rm E}$, in order to compare our results on the same length scale.

3 THE LENSING MODEL

In this section we introduce two gravitational lens models used to measure the total mass of the lensing galaxy within $R_{\rm E}$, $M(< R_{\rm E})$, and to determine the intrinsic properties of the lensed source. We adopt two different lens models: an SIE and a Peudo-Isothermal Elliptical Mass Distribution (PIEMD) (Kassiola & Kovner 1993).

The previous lensing-based studies have demonstrated that the mass density profile of early-type galaxies is consistent with an isothermal mass model, both in the inner regions (within the Einstein radii, see e.g. Lagattuta et al. 2010; Ruff et al. 2011) and at distances of $\sim 50 - 300\ h^{-1}$ kpc (Sheldon et al. 2004; Mandelbaum et al. 2006). Therefore we choose not to constrain the density profile and adopt an SIE model following the normalization proposed by Kormann et al. (1994). The ellipticity ε is related to the axis ratio $q = \sqrt{\frac{1-\varepsilon}{1+\varepsilon}}$ (Keeton & Kochanek 1998). We therefore have three free parameters: the central velocity dispersion (σ), and the shape and orientation of the total mass distribution.

Following recent works (e.g. Jullo et al. 2007), we also model the galaxy with a PIEMD, which is widely used for strong lensing studies both on the scale of a galaxy and the scale of galaxy clusters (Covone et al. 2006; Donnarumma et al. 2009). Five free parameters are included in this model: the core radius (r_0), cut-off radius ($r_{\rm c}$) and velocity dispersion (σ), as well as the shape and orientation of the total mass distribution. As $r_{\rm c}$ vanishes, the potential approaches a singular isothermal potential, truncated at the cut-off radius.

The main lensing galaxy is clearly not isolated: two massive early-type galaxies are found within $\sim 20''$, see Figure 2. These two galaxies are likely members of a galaxy group located along the line of sight at $z \sim 0.7$ (see Sect. 4), which has already been considered in Faure et al. (2011) as a part of the whole lensing system. Therefore, in this section, we consider the contribution of these two massive galaxies to the lensing potential. For simplicity, we have modeled the two additional galaxies as singular isothermal spheres (SISs), with the velocity dispersion as the only free parameter. However, we do not assume *a priori* there is a galaxy group, which can be revealed through the presence of an external shear. Such an external shear allows us to characterize the contribution of the environment to the total lens potential. Therefore, we consider two additional lensing models with two more free parameters: the external shear parametrized by shear strength γ and its orientation PA_γ (two models SIE+SIS+SIS+γ and PIEMD+SIS+SIS+γ, respectively).

Optimization of the lens models has been performed by means of Lenstool (Kneib et al. 1993; Jullo et al. 2007), a tool adopting a Bayesian approach to modeling the process of strong lensing. The best model is obtained by reproducing the location of the observed multiple images (i.e., positions of the brightest peak and shape) within the supplied uncertainties. We also checked that supplying

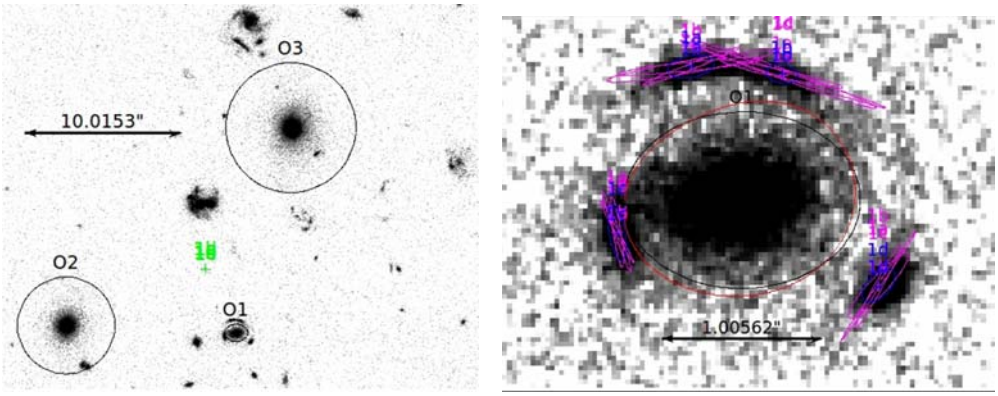

Fig. 2 Mass models with the SIE+SIS+SIS+γ model. *Left panel*: Constraint results with the black circles representing the main galaxy and the source positions of the secondary and tertiary galaxies (these positions are favored and are denoted by green crosses). *Right panel*: Enlarged view of the lens galaxy and the nearby region surrounding it. North is to the top and East to the left. The black circle represents the potential of O1. The blue ellipses are the observed image positions marked by blue text "1a," "1b," "1c" and "1d." The purple ellipses denote the predicted image positions.

Table 1 Positions of the Lensing Galaxy and the Images (in degrees) Used as Constraints for the Lens Mass Model

Lens Image	RA	Dec
COSMOS J095930+023427	149.878930	2.574342
A	149.87902	2.5745776
B	149.87886	2.5745646
C	149.87915	2.5742854
D	149.87869	2.5741922

the expected position of the critical curve between images B and C does not significantly improve the results. We choose to apply a minimization algorithm to the source plane for higher accuracy. In Lenstool, the positions of the images are the observational data that are input to constrain parameters in the lens model. In our analysis, the position of the brightest peak is determined as the image position, and the error in each image position is assumed to be $0.05''$.

In Table 1 we provide the lens galaxy's central coordinates as well as the positions of the multiple images used in the lens modeling. A detailed discussion of the lensing models is given below. We assume the source to be located at redshifts $z = 2$ and 4, when deriving the total mass measurements.

3.1 SIE+SIS+SIS

In order to asses the effect of the external shear produced by the group and cluster, we have utilized two simple models, namely SIE+SIS+SIS and SIE+SIS+SIS+γ.

The main galaxy is described by an SIE, defined by its position, velocity dispersion (σ_1), orientation's position angle (PA) and ellipticity (ε). The SIE central position is fixed to that of the light centroid for the lensing galaxy J095930+023427, as determined in the HST/ACS image. Moreover, considering that there might be a possible misalignment between the luminous bulge and the DM halo (Kochanek 2002), an additional $\pm 20^\circ$ uncertainty is placed on the orientation of the Sersic

Table 2 Best Fit Parameters for the Lens Models Assuming $z_{\rm s} = 2$

Model	$\log E$	χ^2	(γ, PA$_\gamma$)	(σ_1, ε, PA) (km s^{-1})	σ_2 (km s^{-1})	σ_3 (km s^{-1})	$M(< R_{\rm E})$ (10^{11} $M_\odot$)	$f_{\rm DM}(< R_{\rm E})$
(1)	(2)	(3)	(4)	(5)	(6)	(7)	(8)	(9)
SIE+SIS+SIS	–22.06	1.7	–	(238, 0.28, –10°)	391	603	3.49	0.81 ± 0.15
SIE+SIS+SIS+γ	–21.04	2.6	(0.25, +60°)	(231,0.28, +0.52°)	388	600	3.50	0.81 ± 0.15
Model	$\log E$	χ^2	(γ, PA$_\gamma$)	(σ_1, r_0, $r_{\rm c}$) (km s^{-1}, kpc, kpc)	σ_2 (km s^{-1})	σ_3 (km s^{-1})	$M(< R_{\rm E})$ (10^{11} $M_\odot$)	$f_{\rm DM}(< R_{\rm E})$
PIEMD+SIS+SIS	–22.30	1.8	–	(200,0.14,24)	372	596	3.25	0.79 ± 0.12
PIEMD+SIS+SIS+γ	–18.29	5.6	(0.24,+31°)	(199,0.21,37)	373	596	3.24	0.79 ± 0.12

(1) Model name. (2) Bayesian evidence $\log E$. (3) χ^2 of the best lens model. (4) Shear parameters. (5) Best-fit parameters for the main galaxy. (6) Velocity dispersion of galaxy #2. (7) Velocity dispersion of galaxy #3. (8) Mass of the main galaxy in the Einstein radius. (9) DM fraction within the Einstein radius.

bulge's light profile. The prior of the SIE ellipticity is ε=[0.0,0.9], which takes into account the possibility of a shallower distribution for the DM halo (Gavazzi et al. 2007). For the second and third galaxies in the model, we fix the SIS central position to their position in the I-band catalog and the only parameter that varies is the velocity dispersion (σ_2 , σ_3). The external shear is parametrized by two free parameters including a shear strength (γ) and orientation (PA$_\gamma$) with the following priors: γ=[0.0,0.5], PA$_\gamma$=[–90°,90°]. Therefore, the total number of free parameters for the two models is 5 and 7, respectively.

The best-fit values of the model parameters and the values of corresponding Bayesian evidence E and χ^2 (assuming a source located at redshift $z_{\rm s} = 2$) are reported in Table 2. While the quantity $\log E$ can effectively be used to rank lensing models, see Jullo et al. (2007), we report them mainly to show the overall relative quality of the fitted models.

We also recomputed the best-fit models for a source at redshift $z_{\rm s} = 4$, in order to estimate the systematic errors on the DM fractions, as discussed below. From the best-fit model displayed in Figure 2, we see that the fit is (at face value) better when compared with the results of Faure et al. (2011). With additional observational constraints such as the velocity dispersions of the lens galaxy's closest neighbors, it would be possible to obtain a more detailed model of the lens potential which would most probably improve the fit.

The image positions are slightly better reproduced (in terms of χ^2) when an external shear is included in the models (when using both the SIE and PIEMD), as generally expected when both internal and external sources of anisotropy are included in the model. However, the value of the shear strength γ is quite significant since it amounts to about $\gamma \sim 0.2$. Therefore, despite the large shear strength, we shall call this latter model the fiducial lens model in the following, with the results of constraints applied to the model parameters displayed in Table 2 and Figure 2. The total mass of the main galaxy in the Einstein radius would be $M(< R_{\rm E}) = 3.5^{+0.5}_{-0.3} \times 10^{11}\ M_\odot$, a result compatible with that of Faure et al. (2011). We stress here that the velocity dispersion associated with the secondary and tertiary lens could be associated with the galaxy mass, however, we choose not to discuss their masses in this paper, due to the simplifying assumption on the corresponding potential SIS. An improved version of the present mass model will require future measurements of their velocity dispersions. In neither case (with or without external shear), a significant offset between the mass distribution in the lensing model (i.e. the total mass distribution) and the light distribution is found. Indeed, we obtain a value of the ellipticity of the total mass distribution ($\epsilon = 0.28$) that agrees with the ellipticity of the light distribution ($\epsilon = 0.21 \pm 0.05$, see Faure et al. 2011).

Finally, the predicted source positions (for each of the four elliptical images) are given by our fiducial model in Figure 2, and are clearly overlapping with each other. Further constraints and discussion on this lensed galaxy are given in Section 6.

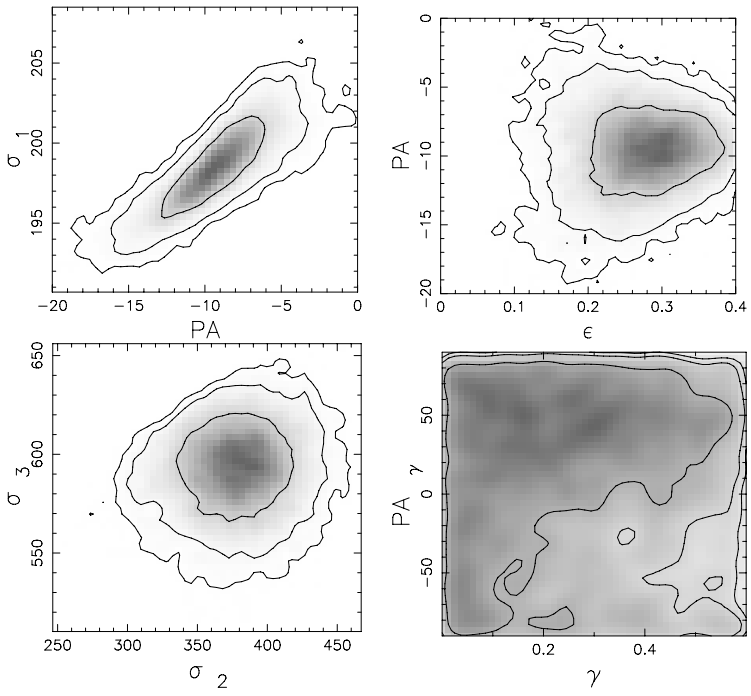

Fig. 3 2D marginalized PDFs for the parameters of the PIEMD+SIS+SIS+γ model. *Top panels*: velocity dispersion of the main galaxy versus galaxy PA; galaxy PA versus ellipticity. *Bottom panels*: velocity dispersion of galaxy #2 and #3; external shear versus shear angle. The three contours represent the 68%, 95% and 99.5% confidence levels.

3.2 PIEMD+SIS+SIS

The lens galaxy model and corresponding mass within the Einstein radius are shown in Table 2, with $M(< R_{\rm E}) = 3.25 \times 10^{11}\ M_{\odot}$. The PIEMD+SIS+SIS+$\gamma$ model yields a similar fit in terms of Bayesian evidence and χ^2, with a relatively large external shear ($\gamma = 0.24$). This clearly supports complementary evidence for the presence of a massive galaxy group located along the line of sight. By using this parametric model again, we also measure an ellipticity with a total mass distribution ($\epsilon = 0.22$) in perfect agreement with that of the light distribution; the DM halo does not appear to be shallower than the stellar distribution.

In Figure 3, we plot the 2D marginalized probability distribution functions (PDFs) for the parameters of the PIEMD+SIS+SIS+γ model. We note that the large value for the velocity dispersion of the most massive galaxy in the lensing system ($\sigma_3 \sim 600\,{\rm km\ s^{-1}}$) can be due to the contribution of the surrounding galaxy groups. In the bottom right panel we show the PDF for the shear parameters. It is evident that these parameters are not as strongly constrained as the other model parameters. While the best-fit value $\gamma = 0.24$ is quite large when compared with estimates of the shear produced by the cosmic environments of strong lensing galaxies (γ ranging from 0.02 to 0.17, Wong et al. 2011), very low values for the shear γ are still well within the 1σ contour. A further study of the present lensing system requires taking into account the detailed galaxy distribution along the line of sight.

3.3 The DM fraction

In this section, we determine the stellar mass within the Einstein radius for the main galaxy, $M_\star(< R_{\rm E})$ and compare it with the total mass within the Einstein radius, $M(< R_{\rm E})$ obtained from lens modeling. Correspondingly, the projected DM fraction within the Einstein radius is obtained: $f_{\rm DM}(< R_{\rm E}) = 1 - \frac{M_\star(<R_{\rm E})}{M(<R_{\rm E})}$. These values are reported in Table 2 when assuming a source is located at $z_{\rm s} = 2$.

The stellar mass is derived following Ilbert et al. (2010) and assuming a Salpeter initial mass function from 0.1 to 100 $M_\odot$. The total stellar mass is found to be $M_* = (0.91 \pm 0.23) \times 10^{11}\, M_\odot$. Hence, the stellar mass inside the Einstein radius can be derived by measuring the light profile, and considering the fraction of the total light inside that radius. We consider here the slight lensing magnification ($\simeq 1.2$) of the galaxy flux by the nearby galaxy group. We obtain $M_*(R_{\rm E}) = 0.68 \pm 0.18 \times 10^{11}\, M_\odot$, slightly smaller than the value found by Faure et al. (2011). We can now use this to determine the DM fraction inside $R_{\rm E}$ and for the whole galaxy. By using the best-fit values given in Table 2 and considering a source located at redshift $z_{\rm s} = 2$, we obtain a value of $f_{\rm DM} = 0.79 \pm 0.12$ (with the PIEMD model). The major source of uncertainty in our lensing model is given by the unknown source redshift. When considering a more distant source at $z_{\rm s} = 4$, we obtain a less massive lensing galaxy. The total mass within the Einstein radius is then measured to be $M(R_{\rm E}) = 2.5 \times 10^{11}\, M_\odot$ and $2.3 \times 10^{11}\, M_\odot$, with the SIE and PIEMD models, respectively, regardless of the external shear. This translates to a lower allowed value for the DM fraction: $f_{\rm DM} = 0.82 \pm 0.12$. While considering the whole galaxy, the DM fraction is 0.95 ± 0.10. Our measurements at ~ 4 effective radii can be directly compared with the findings by Deason et al. (2012), studying a sample of 15 nearby elliptical galaxies, by using planetary nebulae and globular clusters as kinematical tracers. Within 4 $R_{\rm eff}$, the DM fraction is found to be between 0.6 and 0.9, for the galaxy mass range considered here. A large sample at high redshift is required in order to detect any evolution in the DM fraction that arises as a function of galaxy mass.

4 THE PROPERTIES OF THE GALAXY GROUP

As discussed above, a significant external shear in the lensing model points to the presence of a massive structure along the line of sight to the lensing system. This can be combined with other strong evidence for the presence of a galaxy group at $z \sim 0.5$: a spatially extended X-ray emission, and an over-density in the photometric redshift distribution, confirmed by the more sparse spectroscopic data. George et al. (2011) have recently presented a spectroscopic survey of galaxy groups in the redshift range $0 < z < 1$, including this structure.

The analysis of the COSMOS field performed by Finoguenov et al. (2007) allows us to identify galaxy clusters and groups based on their X-ray emissions. The galaxy membership for those groups was assessed in George et al. (2011), based on the distance from the X-ray centroid, as well as photometric and spectroscopic redshifts.

Based on these analyses, Faure et al. (2011) noticed that there is a galaxy group (ID 288 according to the classification in the X-ray and galaxy catalogs) along the line of sight toward our lens, likely to be at $z \sim 0.7$. We use the COSMOS public data[2] to verify the properties of such a group of galaxies.

In Figure 4 we show the HST/ACS I band image of the field around our lens; on the optical image, we overlay the X-ray contours obtained through adaptive smoothing of the 0.5–2 keV Chandra observations of the same region. The adaptive smoothing procedure allows us to separate the emission of the two bright AGNs present in the field from the spatially extended emission likely associated with the galaxy group. Using the most recent versions of the X-ray and galaxy catalogs[3],

[2] *http://irsa.ipac.caltech.edu/data/COSMOS/*

[3] The catalogs are available at *http://astro.berkeley.edu/ mgeorge/cosmos/*

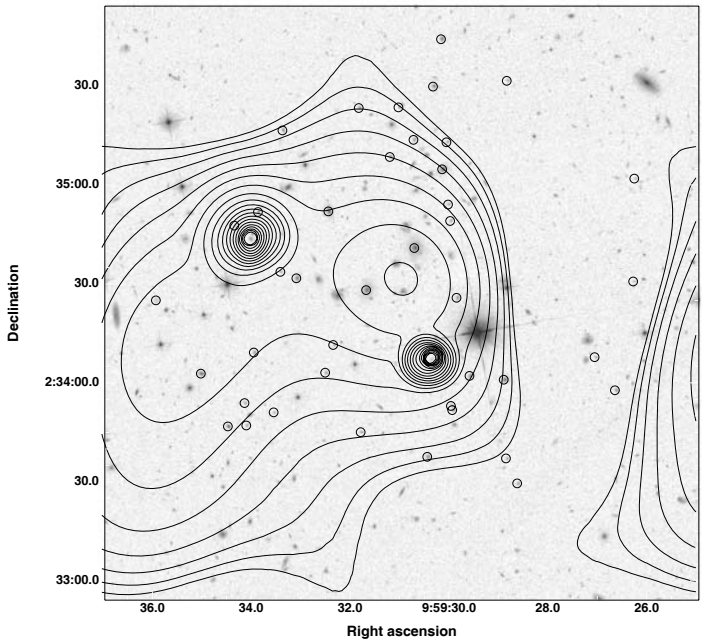

Fig. 4 HST/ACS I band image of the region around the lensing galaxy. The black contours show the X-ray surface brightness distribution in the 0.5–2 keV band, as derived through the adaptive smoothing of the raw X-ray image. Black circles mark the position of the candidate member galaxies of the group, according to the analysis of George et al. (2011).

we identified the galaxies which are candidate group members, and these are shown by the black circles in Figure 4.

Although the X-ray detection has a low significance ($\sim 2\sigma$ as calculated from our adaptively smoothed map, and quality flag 2 in the X-ray catalog), the emission appears to be centered between the two brightest galaxies in the group, and aligned with the main gravitational lens. While the X-ray contours suggest the presence of an eastern tail, which overlaps with the optical group members, the significance of this feature is too low to decide whether it is an artifact of the smoothing process or if it is related to the sparse distribution of the group of galaxies.

To make an independent assessment of the group's mass, we measure the 0.5–2 keV X-ray luminosity within $20''$ (corresponding to a linear scale of 140 kpc at $z = 0.7$) around the X-ray centroid, and derive $L_X = (8.6 - 13) \times 10^{42}$ erg s^{-1} for temperatures in the range $1 - 2$ keV and metallicities $Z/Z_\odot = 0.6 - 1$. Using the scaling relationship provided by Eckmiller et al. (2011), this translates to a mass $M = (3 - 10) \times 10^{13}\ M_\odot$, which is in good agreement with the estimate of $4.4 \times 10^{13}\ M_\odot$ derived by Leauthaud et al. (2011) through weak lensing analysis.

5 THE GALAXY'S STELLAR POPULATION

The lensing galaxy is classified as an early-type galaxy by its morphology, and the basic morphological parameters can be found in the COSMOS Morphology Catalog (v1.1; Cassata et al. 2007). The Sersic index is $n = 1.98 \pm 0.20$, and the effective radius is $\theta_{\rm eff} = 0.21'' \pm 0.08'' \simeq 3.8\,\theta_{\rm E}$. However, the galaxy also shows an evident O[II] emission line, see Figure 5. We measure its luminosity to be $L_{\rm O[II]} = (8.1 \pm 5.9) \times 10^{40}\,{\rm erg\ s^{-1}}$. If interpreting this as a signature of ongoing star-formation,

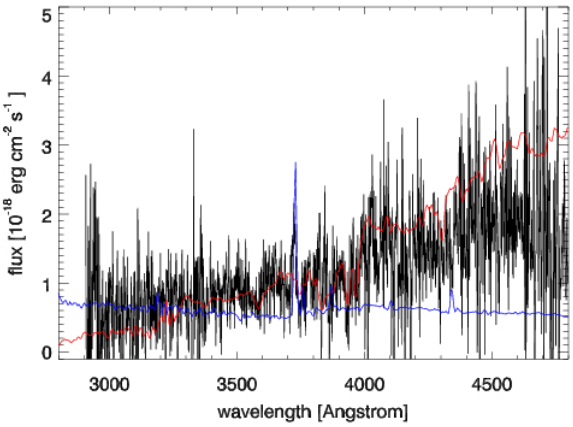

Fig. 5 The optical spectrum of the lensing galaxy from the zCOSMOS project (in black). The [OII] emission line is evident. The observed spectrum is compared with two spectral templates from Kinney et al. (1996): an elliptical galaxy (red) and a star-forming galaxy (blue).

rather than AGN nuclear activity, we can determine the galaxy star-formation rate (SFR) by adopting the calibration introduced by Kennicutt (1998)

$$\mathrm{SFR}\,(M_\odot\ \mathrm{yr}^{-1}) \;=\; 1.4\times10^{-41}\,L(\mathrm{O[II]})\,. \tag{1}$$

We find therefore a modest SFR$\sim 1.2\ M_\odot\ \mathrm{yr}^{-1}$.

We then performed an analysis of the properties of the lensing galaxy's stellar population by using the available low-resolution spectrum from zCosmos and the tool STARLIGHT (Cid Fernandes et al. 2005, 2007). We assume as a base a set of simple stellar populations with a Chabrier (2003) initial mass function, and exclude the wavelength range of the observed emission line. The measured (light-weighted) age of the lensing galaxy is ~ 3.4 Gyr, with the metallicity $Z/Z_0 = 0.014$ ($\chi^2 = 1.5$). Therefore, the galaxy formation epoch is located at redshift $z \sim 2$: however, we caution that this value is to be interpreted as a lower limit, since it is likely that a young stellar population in the galaxy is biasing this measurement.

6 IMAGE RECONSTRUCTION IN THE SOURCE PLANE

Finally, as a demonstration of the capability of the present lensing system as a *gravitational telescope*, we use the lensing model with the lower χ^2 to invert the lensing equation and reconstruct the intrinsic source morphology. With this aim, we used the task `cleanlens` provided by Lenstool (Sharon et al. 2012). For each point of the image plane, the program computes the corresponding point in the source plane.

The inversion result of the HST/ACS I_{814} image is presented in Figure 6. The reconstructed source image allows us to investigate the detailed spatial structure of the magnified source. We find that the galaxy has a scale of about 3.3 kpc at $z_\mathrm{s} = 2$ (2.7 kpc at $z = 4$), and a disturbed disk-like appearance, which is typical in low-mass star-forming galaxies at $z \sim 3$ (Genzel et al. 2011). Unfortunately, the available spectrum shows no clear feature due to the background source (see Fig. 5) and only the HST/ACS image allows a clean separation of the lensed images from the deflector. Therefore deep, spatially resolved spectroscopic data are still required for a large sample of similar lensed sources (magnification ~ 10, $z \sim 3$) to gain further insight into the first stage of galaxy evolution.

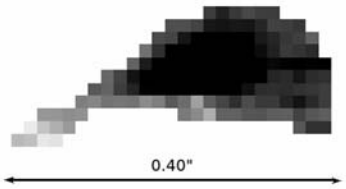

Fig. 6 Image reconstruction of the lensed galaxy, based on the HST/ACS I_{814} data.

7 CONCLUSIONS

We have performed a multi-wavelength analysis of the gravitational lens COSMOS J095930+023427 ($z_{\rm l} = 0.892$), based on the large set of public data from the COSMOS survey. The lensing system is an early-type galaxy with an Einstein radius of $0.79''$. We perform a lensing analysis using both an SIE and a PIEMD. The final results on the total mass, the DM fraction within the Einstein radius and the external shear due to a foreground galaxy group are robust with respect to the choice of the parametric model and the source redshift (yet unknown). We find that the DM fraction is $f_{\rm DM} = 0.75$ at about four effective radii with a source at $z_{\rm s} = 2$, similar to what was recently found in local elliptical galaxies (Deason et al. 2012). The non-null external shear found in our lensing models supports other observational data about the presence and structure of a galaxy group at $z \sim 0.7$, which appears to be centered between the two brightest group galaxies, and aligned with the main gravitational lens according to the X-ray detection. An independent measurement of the 0.5–2 keV X-ray luminosity within $20''$ around the X-ray centroid provides us a group mass of $M = (3 - 10) \times 10^{13}\ M_{\odot}$, a result consistent with the previous estimate derived through weak lensing analysis. We also find that the lensing galaxy shows a strong [OII] emission line, probably due to a low amount of ongoing star-formation activity. Finally, by inverting the lensing equation of the HST/ACS I_{814} image, we obtain the reconstructed source image presented in Figure 6 and investigate the detailed spatial structure of the magnified source. The lensed galaxy has a scale of about 3.3 kpc at $z_{\rm s} = 2$ (2.7 kpc at $z_{\rm s} = 4$), and a typical disturbed disk-like appearance that is common in low-mass star-forming galaxies at $z \sim 3$ (Genzel et al. 2011). However, we note that deep, spatially resolved spectroscopic data for similar lensed sources are still required to detect the first stage of galaxy evolution, since the available spectrum shows no clear features due to the background source (see Fig. 5).

The present multiwavelength study is meant to be the first step in a systematic, individual study of the large sample of gravitational lenses found in the COSMOS field (Faure et al. 2008; Jackson 2008), with the aim to probe the evolution of the structure of the inner regions of elliptical galaxies. A companion spatially-resolved spectroscopic observational campaign is the most natural way to complement the dataset already in hand and obtain a deeper insight into the properties of massive early-type galaxies at $z \sim 0.7 - 1.0$.

Acknowledgements We thank E. Jullo and L. Izzo for helpful discussions. This work is supported by the National Natural Science Foundation of China under the Distinguished Young Scholar program (Grant Nos. 10825313 and 11073005), the National Basic Research Program of China (973 program, Grant No. 2012CB821804), the Fundamental Research Funds for the Central Universities and Scientific Research Foundation of Beijing Normal University, and the Excellent Doctoral Dissertation of Beijing Normal University Engagement Fund.

References

Allam, S. S., Tucker, D. L., Lin, H., et al. 2007, ApJ, 662, L51
Bolton, A. S., Burles, S., Koopmans, L. V. E., Treu, T., & Moustakas, L. A. 2006, ApJ, 638, 703
Bolton, A. S., Burles, S., Koopmans, L. V. E., et al. 2008, ApJ, 682, 964
Cabanac, R. A., Alard, C., Dantel-Fort, M., et al. 2007, A&A, 461, 813
Cao, S., Covone, G., & Zhu, Z.-H. 2012, ApJ, 755, 31
Cao, S., & Zhu, Z.-H. 2012, A&A, 538, A43
Cappellari, M., Bacon, R., Bureau, M., et al. 2006, MNRAS, 366, 1126
Cassata, P., Guzzo, L., Franceschini, A., et al. 2007, ApJS, 172, 270
Chabrier, G. 2003, PASP, 115, 763
Churazov, E., Forman, W., Vikhlinin, A., et al. 2008, MNRAS, 388, 1062
Cid Fernandes, R., Mateus, A., Sodré, L., Stasińska, G., & Gomes, J. M. 2005, MNRAS, 358, 363
Cid Fernandes, R., Asari, N. V., Sodré, L., et al. 2007, MNRAS, 375, L16
Covone, G., Kneib, J.-P., Soucail, G., et al. 2006, A&A, 456, 409
Covone, G., Paolillo, M., Napolitano, N. R., et al. 2009, ApJ, 691, 531
Deason, A. J., Belokurov, V., Evans, N. W., & McCarthy, I. G. 2012, ApJ, 748, 2
Donnarumma, A., Ettori, S., Meneghetti, M., & Moscardini, L. 2009, MNRAS, 398, 438
Eckmiller, H. J., Hudson, D. S., & Reiprich, T. H. 2011, A&A, 535, A105
Faure, C., Kneib, J.-P., Covone, G., et al. 2008, ApJS, 176, 19
Faure, C., Anguita, T., Alloin, D., et al. 2011, A&A, 529, A72
Finoguenov, A., James, B., Peacock, J., et al. 2007, in X-ray Surveys, Evolution of Accretion, Star-Formation and the Large Scale Structure, held 2-6 July, 2007 in Rodos Island, Greece, eds. I. Georgantopoulos, & M. Plionis. Published online at http://www.astro.noa.gr/xray07/, p.59
Gavazzi, R., Treu, T., Rhodes, J. D., et al. 2007, ApJ, 667, 176
Genzel, R., Newman, S., Jones, T., et al. 2011, ApJ, 733, 101
George, M. R., Leauthaud, A., Bundy, K., et al. 2011, ApJ, 742, 125
Grin, D., Covone, G., Kneib, J.-P., et al. 2007, Phys. Rev. D, 75, 105018
Humphrey, P. J., Buote, D. A., Gastaldello, F., et al. 2006, ApJ, 646, 899
Ilbert, O., Salvato, M., Le Floc'h, E., et al. 2010, ApJ, 709, 644
Jackson, N. 2008, MNRAS, 389, 1311
Jullo, E., Kneib, J.-P., Limousin, M., et al. 2007, New Journal of Physics, 9, 447
Kassiola, A., & Kovner, I. 1993, ApJ, 417, 450
Keeton, C. R., & Kochanek, C. S. 1998, ApJ, 495, 157
Kennicutt, R. C., Jr. 1998, ApJ, 498, 541
Kinney, A. L., Calzetti, D., Bohlin, R. C., et al. 1996, ApJ, 467, 38
Kneib, J. P., Mellier, Y., Fort, B., & Mathez, G. 1993, A&A, 273, 367
Kochanek, C. S. 2002, in The Shapes of Galaxies and their Dark Halos, Proceedings of the Yale Cosmology Workshop, ed. P. Natarajan (World Scientific Publishing Co. Pte. Ltd.), 62
Kormann, R., Schneider, P., & Bartelmann, M. 1994, A&A, 284, 285
Lagattuta, D. J., Fassnacht, C. D., Auger, M. W., et al. 2010, ApJ, 716, 1579
Leauthaud, A., Tinker, J., Behroozi, P. S., Busha, M. T., & Wechsler, R. H. 2011, ApJ, 738, 45
Lilly, S. J., Le Brun, V., Maier, C., et al. 2009, ApJS, 184, 218
Mandelbaum, R., Seljak, U., Kauffmann, G., Hirata, C. M., & Brinkmann, J. 2006, MNRAS, 368, 715
Massey, R., Kitching, T., & Richard, J. 2010, Reports on Progress in Physics, 73, 086901
Monna, A., & Covone, G. 2012, Memorie della Societa Astronomica Italiana Supplementi, 19, 258
Moustakas, L. A., Abazajian, K., Benson, A., et al. 2009, in astro2010: The Astronomy and Astrophysics Decadal Survey, Science White Papers, No. 214 (arXiv:0902.3219)

Richard, J., Stark, D. P., Ellis, R. S., et al. 2008, ApJ, 685, 705
Ruff, A. J., Gavazzi, R., Marshall, P. J., et al. 2011, ApJ, 727, 96
Schechter, P. L. 2005, in IAU Symposium, 225, Gravitational Lensing Impact on Cosmology, eds. Y. Mellier, & G. Meylan, 281 (arXiv:astro-ph/0408338)
Scoville, N., Abraham, R. G., Aussel, H., et al. 2007, ApJS, 172, 38
Sharon, K., Gladders, M. D., Rigby, J. R., et al. 2012, ApJ, 746, 161
Sheldon, E. S., Johnston, D. E., Frieman, J. A., et al. 2004, AJ, 127, 2544
Taniguchi, Y., Scoville, N., Murayama, T., et al. 2007, ApJS, 172, 9
Tortora, C., Napolitano, N. R., Romanowsky, A. J., Capaccioli, M., & Covone, G. 2009, MNRAS, 396, 1132
van der Wel, A., & van der Marel, R. P. 2008, ApJ, 684, 260
Walsh, D., Carswell, R. F., & Weymann, R. J. 1979, Nature, 279, 381
Wong, K. C., Keeton, C. R., Williams, K. A., Momcheva, I. G., & Zabludoff, A. I. 2011, ApJ, 726, 84